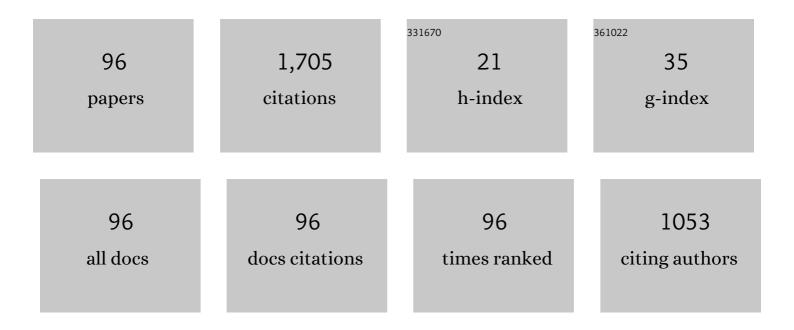
List of Publications by Year in descending order

Source: https://exaly.com/author-pdf/5144316/publications.pdf Version: 2024-02-01



#	Article	IF	CITATIONS
1	Phase selection and solidification path transition of Ti–48Al–xNb alloys with different cooling rates. Rare Metals, 2023, 42, 288-295.	7.1	3
2	Investigations of interfacial reaction and toughening mechanisms of Ta fiber-reinforced TiAl-matrix composites. Materials Characterization, 2022, 183, 111584.	4.4	18
3	Metastable transformation behavior in a Ta-containing TiAl-Nb alloy during continuous cooling. Journal of Alloys and Compounds, 2022, 904, 164088.	5.5	11
4	Phase transformation pathway and microstructural refinement by feathery transformation of Ru-containing Î ³ -TiAl alloy. Journal of Materials Research and Technology, 2022, 18, 5290-5300.	5.8	6
5	High temperature micro-deformation behavior of continuous TiNb fiber reinforced TiAl matrix composite investigated by in-situ high-energy X-ray diffraction. Materials Science & Engineering A: Structural Materials: Properties, Microstructure and Processing, 2022, 846, 143255.	5.6	2
6	Preparation of Al2O3 coating on Nb fiber and the effect on interfacial microstructure of Nbf/TiAl composite. Materials Characterization, 2022, 190, 112061.	4.4	4
7	Portevin-Le Chatelier effect, twinning-detwinning and disordering in an aged Ni–Cr–Mo alloy during large plastic deformation. Materials Science & Engineering A: Structural Materials: Properties, Microstructure and Processing, 2021, 803, 140506.	5.6	5
8	Mechanical properties and microstructure of in situ formed Ti2AlN/TiAl(WMS) composites. Rare Metals, 2021, 40, 190-194.	7.1	8
9	Active Eutectoid Decomposition of α → γ + τ1 and the Morphological Evolution in a Ru-Co Acta Metallurgica Sinica (English Letters), 2021, 34, 1042-1050.	ontaining Ti 2.99	Al Alloy.
10	Microstructure refinement assisted by α-recrystallization in a peritectic TiAl alloy. Journal of Materials Research and Technology, 2021, 11, 1135-1141.	5.8	7
11	Performance assessment of TiNbf/TiAl composites with different fiber structural characteristics. Journal of Materials Research and Technology, 2021, 11, 2265-2276.	5.8	12
12	Plasma electrolytic deposition of α-Al2O3 on TiNb fibres and their mechanical properties. Ceramics International, 2021, 47, 32915-32926.	4.8	6
13	Erosion behaviors and the control of fiber structure in Al2O3,f/TiAl composites. Journal of Alloys and Compounds, 2021, 882, 160734.	5.5	14
14	High temperature micromechanical behavior of Ti2AlN particle reinforced TiAl based composites investigated by in-situ high-energy X-ray diffraction. Materials and Design, 2021, 212, 110225.	7.0	13
15	The phase transformation behavior between Î ³ lamellae and massive Î ³ in a Ta containing TiAl-based alloy. Journal of Alloys and Compounds, 2020, 821, 153290.	5.5	11
16	Continuous-Cooling-Transformation (CCT) Behaviors and Fine-Grained Nearly Lamellar (FGNL) Microstructure Formation in a Cast Ti-48Al-4Nb-2Cr Alloy. Metallurgical and Materials Transactions A: Physical Metallurgy and Materials Science, 2020, 51, 5285-5295.	2.2	16
17	Flexible wire-shaped symmetric supercapacitors with Zn–Co layered double hydroxide nanosheets grown on Ag-coated cotton wire. Journal of Materials Science, 2020, 55, 16683-16696.	3.7	12
18	Evolution and micromechanical properties of interface structures in TiNbf/TiAl composites prepared by powder metallurgy. Journal of Materials Science, 2020, 55, 12421-12433.	3.7	19

#	Article	IF	CITATIONS
19	Grain refinement of 1 at.% Ta-containing cast TiAl-based alloy by cyclic air-cooling heat treatment. Materials Letters, 2020, 274, 127940.	2.6	17
20	Formation mechanism of Si-Y-C ceramic matrix by reactive melt infiltration using Si-Y alloy and properties of C/Si-Y-C composites. Ceramics International, 2020, 46, 18976-18984.	4.8	8
21	Evolution of Metastable α ₂ Phase in a Quenched Highâ€Nb ontaining TiAl Alloy at 800 °C. Advanced Engineering Materials, 2020, 22, 1901539.	3.5	2
22	In-situ observation of microstructure evolution and phase transformation under continuous cooling in Ru-containing TiAl alloys. Materials Characterization, 2020, 163, 110296.	4.4	11
23	Effects of Ru content on phase transformation and compression property of cast TiAl alloys. China Foundry, 2020, 17, 393-401.	1.4	5
24	Sustainable synthesis of N/S-doped porous carbon sheets derived from waste newspaper for high-performance asymmetric supercapacitor. Materials Research Express, 2019, 6, 095605.	1.6	9
25	Refinement of massive γ phase with enhanced properties in a Ta containing γ-TiAl-based alloys. Scripta Materialia, 2019, 172, 113-118.	5.2	42
26	Microstructural evolution and creep deformation behavior of novel Tiâ^'22Alâ^'25Nbâ^'1Moâ^'1Vâ^'1Zrâ^'0.2Si (at.%) orthorhombic alloy. Transactions of Nonferrous Metals Society of China, 2019, 29, 313-321.	4.2	18
27	A Newly Generated Nearly Lamellar Microstructure in Cast Ti-48Al-2Nb-2Cr Alloy for High-Temperature Strengthening. Metallurgical and Materials Transactions A: Physical Metallurgy and Materials Science, 2019, 50, 5839-5852.	2.2	23
28	Catalytic effect of EG and MoS ₂ on hydrolysis hydrogen generation behavior of highâ€energy ballâ€milled Mgâ€10wt.%Ni alloys in NaCl solution—A powerful strategy for superior hydrogen generation performance. International Journal of Energy Research, 2019, 43, 8426.	4.5	12
29	Enhanced hydrogen generation behaviors and hydrolysis thermodynamics of as-cast Mg–Ni–Ce magnesium-rich alloys in simulate seawater. International Journal of Hydrogen Energy, 2019, 44, 24086-24097.	7.1	40
30	Microstructure evolution and controlled hydrolytic hydrogen generation strategy of Mg-rich Mg-Ni-La ternary alloys. Energy, 2019, 188, 116081.	8.8	40
31	On the eutectoid decomposition of α→γ+τ1 in a Ru-containing TiAl alloy. Journal of Alloys and Compounds, 2019, 790, 42-47.	5.5	8
32	Facile synthesis of mesoporous CuCo2O4 nanorods@MnO2 with core-shell structure grown on RGO for high-performance supercapacitor. Materials Letters, 2019, 249, 151-154.	2.6	20
33	Continuous cooling transformationÂ(CCT) behavior of a high Nb-containing TiAl alloy. Materialia, 2019, 5, 100169.	2.7	13
34	Microstructure evolution and mechanical properties of a Ti-45Al-8.5Nb-(W, B, Y) alloy obtained by controlled cooling from a single Î ² region. Journal of Alloys and Compounds, 2018, 740, 1140-1148.	5.5	25
35	Nucleation behavior of ωo phase in TiAl alloys at different elevated temperatures. Journal of Materials Science, 2018, 53, 5287-5295.	3.7	5
36	Generation of high-performance Ni-Cr-Mo-based superalloys via Î ³ to DO22 superlattice ordered phase transformation upon addition of trace alloying elements. Materials Science & Engineering A: Structural Materials: Properties, Microstructure and Processing, 2018, 738, 38-43.	5.6	10

#	Article	IF	CITATIONS
37	The effect of Ni3(Cr0.2W0.4Ti0.4) particles with DO22 structure on the deformation mode and mechanical properties of the aged Ni-Cr-W-Ti alloy. Scripta Materialia, 2018, 153, 44-48.	5.2	12
38	Competitive growth of Si and YSi2 phases in a eutectic Si-Y alloy prepared by the Bridgeman method. Ceramics International, 2018, 44, 13232-13239.	4.8	6
39	Modification based on internal refinement and external decoration: A powerful strategy for superior thermodynamics and hysteresis of Mg-Ni hydrogen energy storage alloys. Journal of Alloys and Compounds, 2018, 766, 112-122.	5.5	30
40	Mechanical properties of an aged Ni-Cr-Mo alloy and effect of long-range order phase on deformation behavior. Materials Science & Engineering A: Structural Materials: Properties, Microstructure and Processing, 2018, 731, 29-35.	5.6	8
41	Anomalous Tensile Strength and Fracture Behavior of Polycrystalline Iridium from Room Temperature to 1600 °C. Advanced Engineering Materials, 2018, 20, 1701114.	3.5	3
42	High-temperature rotary-bending fatigue characteristics of a high Nb-containing beta-gamma TiAl alloy. Materials Science & Engineering A: Structural Materials: Properties, Microstructure and Processing, 2018, 735, 40-48.	5.6	14
43	Oxidation behavior of a novel multi-element alloyed Ti2AlNb-based alloy in temperature range of 650–850°C. Rare Metals, 2018, 37, 838-845.	7.1	17
44	Formation of nano-sized M2C carbides in Si-free GH3535 alloy. Scientific Reports, 2018, 8, 8158.	3.3	10
45	Hot corrosion behavior and mechanical properties degradation of a Ni–Cr–W-based superalloy. Rare Metals, 2017, 36, 23-31.	7.1	6
46	The Effect of Pressure Stress on the Evolution of B2(ï‰) Phase in High Nb Containing TiAl Alloy. Advanced Engineering Materials, 2017, 19, 1600844.	3.5	7
47	The effect of Ti on precipitation of fully coherent DO 22 superlattice in an Ni-Cr-W-based superalloy. Scripta Materialia, 2017, 134, 15-19.	5.2	18
48	Tailoring the Microstructure of a β-Solidifying TiAl Alloy by Controlled Post-solidification Isothermal Holding and Cooling. Metallurgical and Materials Transactions A: Physical Metallurgy and Materials Science, 2017, 48, 5095-5105.	2.2	32
49	Isothermal activation, thermodynamic and hysteresis of MgH2 hydrides catalytically modified by high-energy ball milling with MWCNTs and TiF3. International Journal of Hydrogen Energy, 2017, 42, 22953-22964.	7.1	28
50	Evolution of Σ3n CSL boundaries in Ni-Cr-Mo alloy during aging treatment. Materials Characterization, 2017, 134, 379-386.	4.4	9
51	Tensile properties and fracture behavior of in-situ synthesized Ti 2 AlN/Ti48Al2Cr2Nb composites at room and elevated temperatures. Materials Science & Engineering A: Structural Materials: Properties, Microstructure and Processing, 2017, 679, 7-13.	5.6	55
52	Effects of hot compression on carbide precipitation behavior of Ni—20Cr—18W—1Mo superalloy. Transactions of Nonferrous Metals Society of China, 2016, 26, 2883-2891.	4.2	5
53	Portevin-Le Chatelier effect in a Ni–Cr–Mo alloy containing ordered phase with Pt2Mo-type structure at room temperature. Materials Science & Engineering A: Structural Materials: Properties, Microstructure and Processing, 2016, 650, 317-322.	5.6	11
54	Microstructure stability of Ti2AlN/Ti–48Al–2Cr–2Nb composite at 900 °C. Transactions of Nonferrous Metals Society of China, 2016, 26, 423-430.	4.2	14

#	Article	IF	CITATIONS
55	Microstructure determined fracture behavior of a high Nb containing TiAl alloy. Materials Science & Engineering A: Structural Materials: Properties, Microstructure and Processing, 2016, 666, 297-304.	5.6	28
56	Evolution behavior of superlattice phase with Pt ₂ Mo-type structure in Ni–Cr–Mo alloy with low atomic Mo/Cr ratio. Journal of Materials Research, 2016, 31, 427-434.	2.6	6
57	Effect of Nb Content on Solidification Characteristics and Microsegregation in Cast Ti–48Al–xNb Alloys. Acta Metallurgica Sinica (English Letters), 2016, 29, 714-721.	2.9	8
58	Microstructure evolution during the precipitation and growth of fully coherent DO22 superlattice in an Ni-Cr-W alloy. Materials Characterization, 2016, 118, 244-251.	4.4	10
59	Microstructural refinement of Ni-Cr-W superalloy by isothermal treatment near the liquidus. Materials Letters, 2016, 175, 271-274.	2.6	7
60	Precipitation of two kinds of γ laths in massive γ coexisting with γ lamellae in as-cast Ta-containing TiAl-Nb alloys. Materials Letters, 2016, 185, 480-483.	2.6	7
61	Correlation between mechanism of ordering transformation and microstructure of interfaces in Ni-Cr-W superalloys. Materials Letters, 2016, 181, 63-66.	2.6	3
62	Elements segregation and phase precipitation behavior at grain boundary in a Ni-Cr-W based superalloy. Materials Characterization, 2016, 122, 189-196.	4.4	30
63	Ordering Transformation and Age Hardening in a Ni-Cr-W Superalloy. Metallurgical and Materials Transactions A: Physical Metallurgy and Materials Science, 2016, 47, 5907-5917.	2.2	5
64	Grain boundary character correlated carbide precipitation and mechanical properties of Ni-20Cr-18W-1Mo superalloy. Materials Science & Engineering A: Structural Materials: Properties, Microstructure and Processing, 2016, 667, 391-401.	5.6	29
65	Transition of solidification path in nonequilibrium solidification of Ti–48Al–8Nb alloy. Rare Metals, 2016, 35, 48-53.	7.1	0
66	Dendritic Growth and Microstructure Evolution with Different Cooling Rates in Ti48Al2Cr2Nb Alloy. Journal of Materials Engineering and Performance, 2016, 25, 38-45.	2.5	16
67	New insights into serrated flow in Pt 2 Mo-type superlattice strengthened Ni–Cr–Mo alloy at room temperature. Materials Letters, 2016, 163, 94-97.	2.6	15
68	Hydrogenation thermodynamics of melt-spun magnesium rich Mg–Ni nanocrystalline alloys with the addition of multiwalled carbon nanotubes and TiF3. Journal of Power Sources, 2016, 306, 437-447.	7.8	66
69	Precipitation of coherent Ni2(Cr, W) superlattice in an Ni–Cr–W superalloy. Materials Characterization, 2016, 111, 86-92.	4.4	5
70	Heredity of medium-range order structure from melts to the microstructure of Ni–Cr–W superalloy. Applied Physics A: Materials Science and Processing, 2015, 120, 183-188.	2.3	6
71	Microstructure and electrochemical hydrogenation/dehydrogenation performance of melt-spun La-doped Mg2Ni alloys. Materials Characterization, 2015, 106, 163-174.	4.4	29
72	Hot corrosion characteristics of Ni–20Cr–18W superalloy in molten salt. Transactions of Nonferrous Metals Society of China, 2015, 25, 3840-3846.	4.2	20

#	Article	IF	CITATIONS
73	Widmannstäten laths in Ti48Al2Cr2Nb alloy by undercooled solidification. Materials Characterization, 2015, 107, 156-160.	4.4	16
74	A mixture of massive and feathery microstructures of Ti48Al2Cr2Nb alloy by high undercooled solidification. Materials Characterization, 2015, 100, 104-107.	4.4	22
75	Precipitation Behavior of σ-FeCr Phases in Hastelloy C-2000 Superalloy Under Plastic Deformation and Aging Treatment. Journal of Materials Engineering and Performance, 2015, 24, 565-571.	2.5	3
76	Oxidation behavior of Hastelloy C-2000 superalloy at 800 °C and 1000 °C. Transactions of Nonferrous Metals Society of China, 2015, 25, 354-362.	4.2	6
77	Effects of β-Dendrite Growth Velocity on βÂ→Âα Transformation of Hypoperitectic Ti–46Al–7Nb Alloy. Acta Metallurgica Sinica (English Letters), 2015, 28, 58-63.	2.9	0
78	Mechanical properties and pore structure deformation behaviour of biomedical porous titanium. Transactions of Nonferrous Metals Society of China, 2015, 25, 1543-1550.	4.2	35
79	Solidification characteristics of high Nb-containing γ-TiAl-based alloys with different aluminum contents. Rare Metals, 2015, 34, 381-386.	7.1	17
80	Microstructural stability of long term aging treated Ti–22Al–26Nb–1Zr orthorhombic titanium aluminide. Transactions of Nonferrous Metals Society of China, 2015, 25, 2549-2555.	4.2	12
81	Corrosion Behavior of Ni–20Cr–18W–1Mo Superalloy in Supercritical Water. Acta Metallurgica Sinica (English Letters), 2014, 27, 1046-1056.	2.9	4
82	Microstructure Characterization and Mechanical Properties of In Situ Synthesized Ti ₂ <scp>A</scp> I <scp>N</scp> / <scp>T</scp> i48 <scp>A</scp> I2 <scp>C</scp> r2 <scp>N</scp> b Composites. Advanced Engineering Materials, 2014, 16, 507-510.	3.5	17
83	Hydrogen desorption performance of high-energy ball milled Mg 2 NiH 4 catalyzed by multi-walled carbon nanotubes coupling with TiF 3. International Journal of Hydrogen Energy, 2014, 39, 19672-19681.	7.1	51
84	Precipitation Behavior of Pt2Mo-Type Superlattices in Hastelloy C-2000 Superalloy with Low Mo/Cr Ratio. Journal of Materials Engineering and Performance, 2014, 23, 3314-3320.	2.5	7
85	Structure, composition and morphology of bioactive titanate layer on porous titanium surfaces. Applied Surface Science, 2014, 308, 1-9.	6.1	20
86	Precipitation of nanosized DO22 superlattice with high thermal stability in an Ni–Cr–W superalloy. Scripta Materialia, 2014, 76, 49-52.	5.2	18
87	Hydrogenation behavior of high-energy ball milled amorphous Mg2Ni catalyzed by multi-walled carbon nanotubes. International Journal of Hydrogen Energy, 2013, 38, 16168-16176.	7.1	21
88	Mechanical properties of porous titanium with different distributions of pore size. Transactions of Nonferrous Metals Society of China, 2013, 23, 2317-2322.	4.2	57
89	Synergetic catalytic effect of MWCNTs and TiF3 on hydrogenation properties of nanocrystalline Mg-10wt%Ni alloys. International Journal of Hydrogen Energy, 2013, 38, 12904-12911.	7.1	20
90	Precipitation behavior of grain boundary M23C6 and its effect on tensile properties of Ni–Cr–W based superalloy. Materials Science & Engineering A: Structural Materials: Properties, Microstructure and Processing, 2012, 548, 83-88.	5.6	119

#	Article	IF	CITATIONS
91	Microstructure evolution in undercooled Co80Pd20 alloys. Journal of Materials Science, 2011, 46, 5495-5502.	3.7	5
92	Effect of thermal exposure on the stability of carbides in Ni–Cr–W based superalloy. Materials Science & Engineering A: Structural Materials: Properties, Microstructure and Processing, 2011, 528, 2339-2344.	5.6	61
93	Stress induced deformation in the solidification of undercooled Co80Pd20 alloys. Materials Science & Engineering A: Structural Materials: Properties, Microstructure and Processing, 2011, 528, 973-977.	5.6	22
94	Effect of temperature on tensile behavior of Ni–Cr–W based superalloy. Materials Science & Engineering A: Structural Materials: Properties, Microstructure and Processing, 2011, 528, 1974-1978.	5.6	79
95	Hot working characteristic of as-cast and homogenized Ni–Cr–W superalloy. Materials Science & Engineering A: Structural Materials: Properties, Microstructure and Processing, 2009, 508, 141-147.	5.6	36
96	Interface morphology evolvement and microstructure characteristics of hypoeutectic Cu–1.0 wt%Cr alloy during unidirectional solidification. Science and Technology of Advanced Materials, 2005, 6, 950-955.	6.1	5